Applied Clay Science 232 (2023) 106793

Contents lists available at ScienceDirect

Applied Clay Science

journal homepage: www.elsevier.com/locate/clay

Geochemistry and palaeo-hydrogeology of the weathered zone in the Opalinus Clay

Martin Mazurek [a,*], Paul Wersin [a], Jebril Hadi [a], Jean-Marc Grenèche [b], Nouvarat Prinpreecha [a], Daniel Traber [c]

[a] Institute of Geological Sciences, University of Bern, Switzerland
[b] Institut des Molécules et Matériaux du Mans, IMMM UMR CNRS 6283, Université du Maine, France
[c] Nagra, Wettingen, Switzerland

ARTICLE INFO

Keywords:
Shale
Pore water composition
Oxidation
Redox buffering
Diffusion
Fracture flow

ABSTRACT

The effects of weathering and decompaction on the Opalinus Clay in northern Switzerland were studied on the basis of a 146 m long drillcore profile. Below 6 m of Quaternary sediments, the rock down to 16 m depth is affected by partial or complete dissolution of siderite, calcite, pyrite and organic matter, with goethite as the only identified product. The reduction level of Fe (Fe^{2+}/Fe_{tot}) in the rock increases with depth from <20% to >80% in unweathered rock below 24 m. Porosity reaches 0.39 in the shallowest samples before dropping to normal values of around 0.13 below 30 m. Pore-water composition obtained by rock squeezing evolves with depth from fresh water of the Ca-SO_4-HCO_3 type to a 10–12 g/L Na-SO_4-Cl type in unweathered rock below 40 m. Ground-water samples taken in the weathered zone indicate reducing conditions at present and therefore reflect a remaining redox buffering capacity even in the strongly oxidised rock. The interpretation of the rock properties, in conjunction with the chemical and isotopic signatures of ground and pore waters, suggests that substantial weathering occurred primarily during stages with a lower ground-water table in the Pleistocene, providing access to oxygen via gas diffusion across the partially unsaturated zone. Three evolutionary stages can be distinguished: 1) Long-term pyrite oxidation during Pleistocene surface exposure under dry climate and diffusive transport of SO_4^{2-} into the formation. This explains the higher SO_4^{2-} pore-water concentrations even in the unweathered rock at depth when compared to regional data from deep boreholes. 2) Build-up of the curved Cl^- and water-isotope diffusion profiles since ~50–60 ka with a depth penetration of 40–80 m. 3) Holocene rise of the water table, leading to self sealing of fractures and the establishment of a diffusive regime in the weathered zone. Under saturated conditions, the depth penetration of rock oxidation is quite limited, which illustrates the substantial buffering capacity of the Opalinus Clay against external geochemical disturbances.

1. Introduction

Clays and mudstones are known to have extremely low hydraulic conductivity, and solute transport at depth is dominated by diffusion (Neuzil, 1994, 2019; Mazurek et al., 2011). However, the mechanical and transport properties may change substantially when, after basin inversion, a clay-rich formation is uplifted. Fracture networks may develop in over-consolidated mudstones due to decompaction and desaturation close to the surface (e.g. Wetzel and Einsele, 1991; Mertens et al., 2003), with potentially drastic effects on transport properties. Fracture flow may trigger the infiltration of oxygenated meteoric water and lead to various types of wallrock alteration (Wetzel and Einsele, 1991; Mazurek et al., 1996; Mäder and Mazurek, 1998; Bao et al., 2017; Lerouge et al., 2018; Le Meur et al., 2021).

In a study targeted at tunnels across the Opalinus Clay in the Swiss Jura Fold-and-Thrust Belt, Gautschi (2001) concluded that, in spite of a high degree of deformation, no water inflows or moisture zones exist at depths exceeding 200 m below surface, whereas at shallower levels, fractures may be water-conducting. Hekel (1994) investigated a number of boreholes into the outcropping Opalinus Clay in southern Germany and identified hydraulic conductivities of 1×10^{-6} m/s or higher in the uppermost 10–30 m, whereas the values dropped by several orders of magnitude below this level. In the same boreholes, the Cl^- content of the pore water of the Opalinus Clay was also reduced in the uppermost

* Corresponding author.
E-mail address: mazurek@geo.unibe.ch (M. Mazurek).

https://doi.org/10.1016/j.clay.2022.106793
Received 23 August 2022; Received in revised form 22 November 2022; Accepted 30 November 2022

20–50 m due to advective and/or diffusive exchange with meteoric water.

In this study, we investigate the physical, geochemical and mineralogical effects of decompaction on the Opalinus Clay in northern Switzerland. The main objectives of the study include the characterisation of the formation in a near-surface position regarding rock/water interactions (such as oxidation), pore-water composition and the effects of decompaction (such as rock deformation, changes of permeability and matrix porosity). Particular attention is given to the characterisation of Fe-bearing minerals in the surficial oxidation zone and the investigation of pore-water composition as a function of depth. Profiles of conservative pore-water tracers, such as Cl^- and stable water isotopes, are modelled, in order to quantify the time scales necessary to establish the currently observed compositions.

The applied aspects of the study pertain to deep geological disposal of radioactive waste, where time scales of 1 Myr or more into the future are considered in safety assessments (NEA, 2009). Over such long periods, a repository may be exhumed due to uplift and erosion. While most of the activity related to fission and activation products has long decayed by then, some long-lived nuclides will still be present, in particular ^{235}U and ^{238}U. Given the fact that U is mobile under oxidising conditions, the extent and the characteristics of the weathered Opalinus Clay (the host rock selected in Switzerland) are of interest.

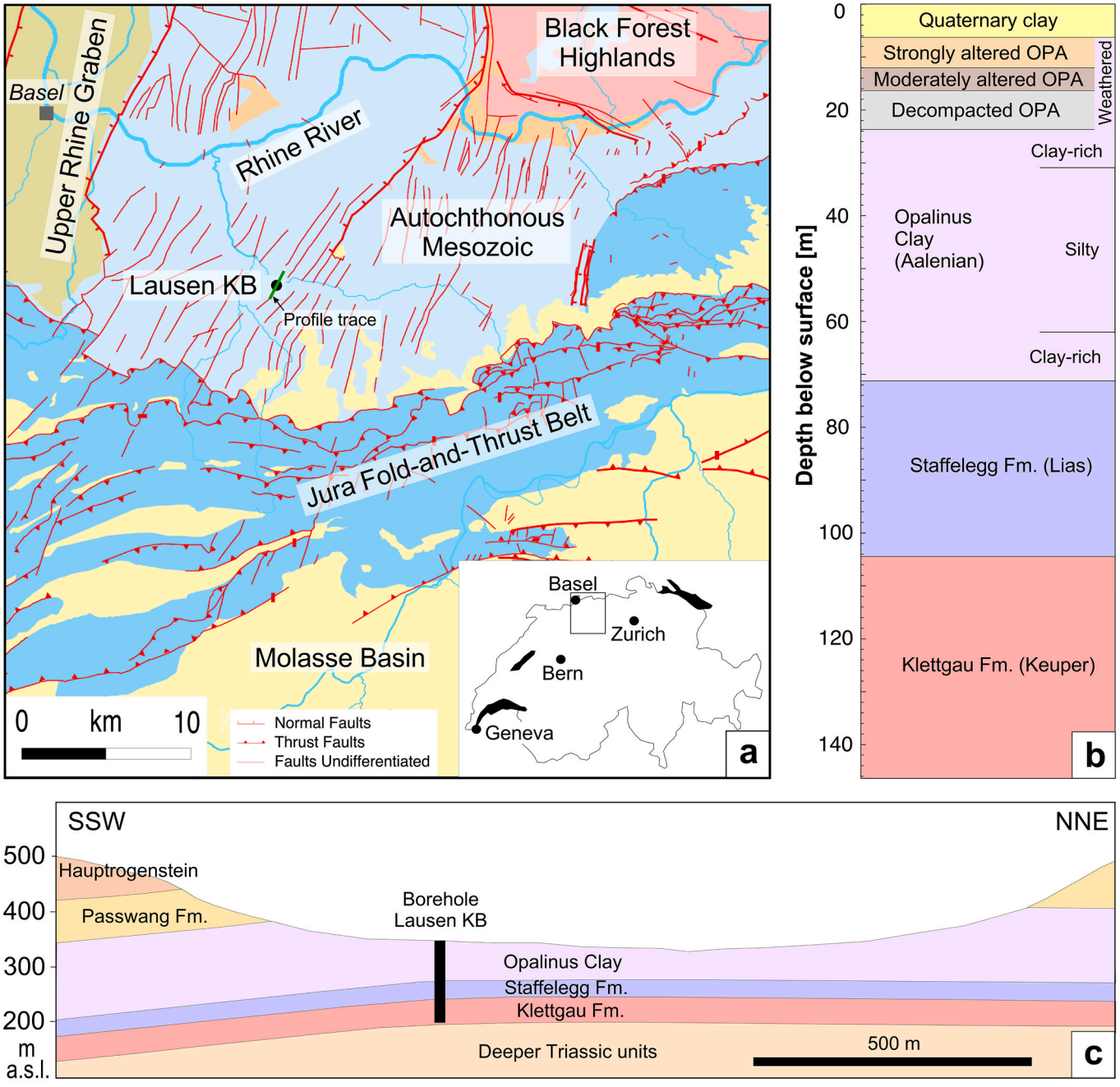

Fig. 1. Geological setting of the Lausen KB borehole.
a. Tectonic map and geographic localisation
b. Schematic drillcore profile
c. Geological profile, modified after Vogt et al. (2017). Green line in a. shows the profile trace

2. Geological setting

Borehole Lausen KB (Swiss coord. 2′624’157/1′257’719/345) was drilled as a geothermal probe in October 2015 to a depth of 146.53 m in the Tabular Jura (autochthonous Mesozoic cover rocks) of northwestern Switzerland. It is located in a topographic low (Ergolz Valley) where the Opalinus Clay crops out at the surface (Fig. 1a, c). Details about on-site operations and field results are documented in Vogt et al. (2016, 2017). A simplified profile of the fully cored borehole is shown in Fig. 1b, and a basic characterisation is provided in Mazurek et al. (2017a).

The Opalinus Clay is an Aalenian (170–174 Ma) formation that occurs throughout northern Switzerland and southern Germany with a thickness in the range 80–120 m (Wetzel and Allia, 2003). Its lithological heterogeneity is remarkably limited over the region. On average, it consists of 60 ± 12 wt% clay minerals (illite, illite/smectite mixed layers, kaolinite, chlorite), 22 ± 6 wt% quartz and feldspars, 13 ± 10 wt % calcite and minor contributions of siderite, pyrite and organic matter (Mazurek, 2011). In the vertical dimension, lithological sub-units, reflecting slight variations in sedimentary facies, were defined by Lauper et al. (2021). Owing to maximum burial in the Cretaceous and subsequent basin inversion (Mazurek et al., 2006; Giger et al., 2015), the Opalinus Clay is an indurated and over-consolidated shale.

At the Lausen site, the Opalinus Clay is covered by 6.22 m soft Quaternary sediment, consisting of brownish loam with limestone fragments from overlying strata, as well as sandy or mica-rich sections (Vogt et al., 2017). The total thickness of the underlying Opalinus Clay is 65 m, which means that the uppermost 35–55 m have been eroded. The upper- and lowermost, clay-rich parts of the formation are separated by a more silty sub-unit between 31 and 62 m. The Opalinus Clay is underlain by the lithologically more heterogeneous Staffelegg Fm. (Liassic; marls, siltstones, limestones) and the Klettgau Fm. (Keuper; dolomitic mudstones to dolostones).

While the site has never been glaciated during the last glacial period, the most extensive glaciation (Möhlin phase, 500 ± 100 ka; Dieleman et al., 2022) covered the site, even though the ice front reached only a few km beyond the site and was likely thin (Kelly et al., 2004; Keller and Krayss, 2010; Preusser et al., 2011).

3. Results and discussion of rock studies

Descriptions of methodology are documented in the Supplementary materials.

3.1. Macroscopic characteristics and porosity of the weathered zone

Below the Quaternary cover, in the interval 6.22–12.03 m, the Opalinus Clay is strongly altered, soft, fractured and has a brownish colour. Bedding is obliterated to a substantial degree. In the underlying section 12.03–16.37 m, a moderate degree of alteration is found. Here, the core is still soft and fractured but the colour is darker and more greyish. Bedding and rock texture are recognisable, often well preserved. Below 15.39 m, the whole rock matrix is grey, while localised oxidation still occurs along fractures (Fig. 2a). The interval 16.37–23.65 m is termed “decompaction zone” and is devoid of macroscopically visible rock alteration, but the degree of fracturing remains high (Fig. 2b). Below 23.65 m, the rock shows no evident effects of weathering, except for a fracture density that is enhanced to a depth of ca. 40 m when compared to the underlying part of the profile.

The thickness of the strongly weathered zone in Lausen is 6 m, which is on the upper end of the range of 1.5–6 m observed by Hekel (1994) on the basis of 18 borehole profiles in southern Germany. There, a Quaternary cover consisting of transported sediment is mostly missing, in contrast to the 6 m observed at Lausen.

Porosity data were obtained from density measurements, from water

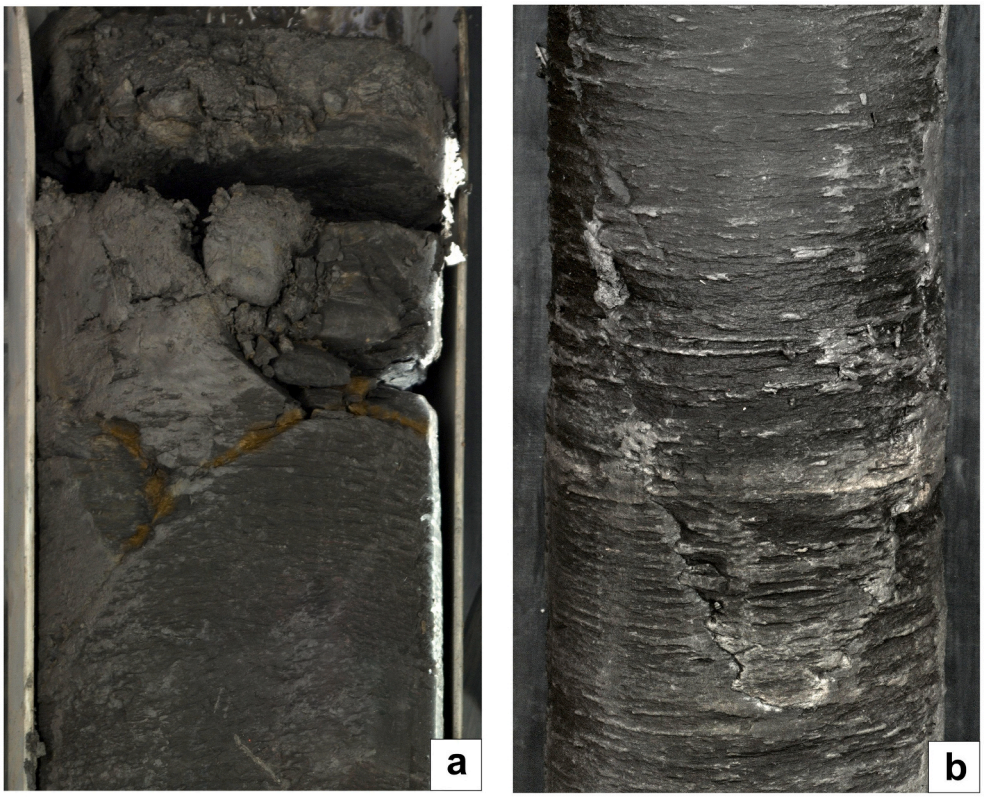

Fig. 2. Core photographs of fractures in the weathered zone. Width of core is 10 cm.
a. Discordant fracture at 15.76–15.94 m depth with brownish alteration rims due to the presence of goethite
b. Discordant, potentially water-conducting fracture at 19.70–19.92 m depth

loss at 105 °C and from mass balance based on water-isotope data using the diffusive exchange method (Rübel et al., 2002). The results of all methods are listed in Table 1. As illustrated in Fig. 3, results from all methods are consistent. At depth, porosity lies around 0.13, a typical value for the Opalinus Clay from deep boreholes (Nagra, 2014). In the uppermost 30–40 m, it increases substantially towards the surface and reaches almost 0.4 in the shallowest sample. Such an impressive increase is also facilitated by the fact that the Opalinus Clay is only poorly cemented and contains swelling clay minerals. It is also worth noting that the zone with increased porosity reaches well below the weathered zone. This means that the mechanical effect of decompaction reaches deeper than the geochemical effects of weathering.

3.2. Mineralogical composition

Results of mineralogical analyses are listed in Table 2, and depth trends for selected minerals are shown graphically in Fig. S1 (Supplementary materials) for the weathered zone and the upper clay-rich subunit (the underlying silty sub-unit [see Fig. 1b] has a somewhat different primary mineralogy and so is not directly comparable). The following observations can be made:

- Only the uppermost 2 samples (down to 8.23 m) show reduced contents of organic carbon. In the case of pyrite, the uppermost 3 samples (down to 8.58 m) are strongly depleted.
- As the oxidation of pyrite or organic matter produces H^+, some carbonate dissolution would be expected. Indeed, calcite and dolomite show decreasing trends towards the surface but are not completely dissolved (except for dolomite in some samples from the strongly altered zone). On the other hand, siderite is quantitatively removed in the strongly altered zone.
- Thus, mineral dissolution affects mainly carbonate phases, pyrite and organic matter, whereas silicate minerals are not affected (apart from the oxidation of chlorite).
- Goethite is the only identified solid product of weathering. It is present in the strongly weathered zone and, in reduced quantity, also in the moderately altered zone.
- The variability of total clay minerals and quartz in the weathered zone is considered to be a primary feature, augmented to some degree by passive enrichment due to the dissolution of carbonates.
- Clay minerals include illite, illite/smectite mixed-layers, kaolinite and chlorite. The only difference between the XRD patterns of unweathered and altered rocks is identified in the uppermost two samples (7.83 and 8.58 m). Here, the higher ratio of the 001 to 003 peaks is taken as evidence of partial oxidation (see Borggaard et al., 1982). Further, the 001 peak shifts to a slightly higher d value upon glycolation, indicative of a swelling smectitic component.

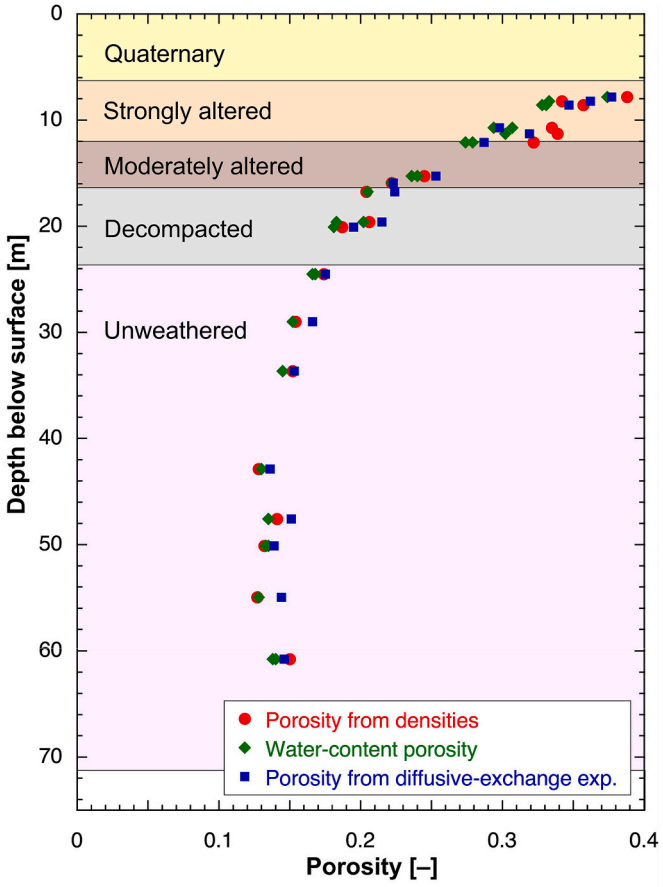

Fig. 3. Porosity profile based on 3 different methods. Background colours correspond to those of Fig. 1b.

It is observed that mineral reactions were extensive in the strongly altered zone but are much less developed in the moderately altered zone. The depth to which individual phases are affected by weathering is mineral-dependent. While pyrite and, even more so, organic matter are markedly affected only in the uppermost ca. 2 m of the Opalinus Clay, quantitative siderite dissolution reaches to a depth of 12 m (base of the

Table 1
Results of density and porosity determinations.

Depth [m]	Unit	Grain density [g/cm^3]	Bulk wet density [g/cm^3]	Porosity from densities [–]	Water-content porosity [–]	Porosity from diff. exch. [–]
7.83		2.702	2.019	0.388	0.374	0.377
8.23		2.694	2.100	0.342	0.333	0.362
8.58	Strongly altered Opalinus Clay	2.682	2.042	0.357	0.331	0.347
10.73		2.691	2.083	0.335	0.307	0.298
11.30		2.689	2.063	0.339	0.302	0.319
12.10	Moderately altered Opalinus Clay	2.680	2.074	0.322	0.274	0.287
15.28		2.683	2.258	0.245	0.236	0.253
15.94		2.692	2.315	0.222	0.222	0.223
16.75		2.702	2.355	0.204	0.205	0.224
19.62	Decompacted Opalinus Clay	2.705	2.325	0.206	0.183	0.215
20.09		2.689	2.364	0.187	0.181	0.195
24.52		2.719	2.412	0.174	0.168	0.175
29.02		2.701	2.436	0.154	0.152	0.166
33.65		2.715	2.445	0.152	0.145	0.153
42.88	Unweathered Opalinus Clay	2.697	2.484	0.128	0.130	0.136
47.58		2.710	2.462	0.141	0.135	0.151
50.13		2.711	2.490	0.132	0.135	0.139
54.98		2.726	2.507	0.127	0.128	0.144
60.78		2.692	2.424	0.150	0.138	0.146

Table 2
Mineralogical composition of whole rocks based on X-ray diffraction and CNS analysis.

Depth [m]	Unit	Calcite [wt%]	Dolomite / Ankerite [wt %]	Siderite [wt%]	Quartz [wt%]	Albite [wt%]	K-feldspar [wt%]	Pyrite [wt%]	C(org) [wt%]	Total clay minerals incl. goethite [wt%]	Goethite [wt%]	Illite [wt%]	I-Sm mixed layers [wt %]	Chlorite [wt%]	Kaolinite [wt%]
7.83		4	b.d.	b.d.	21	0.5	3	0.1	0.7	71	4	21	16	9	20
8.23		4	0.5	b.d.	24	0.5	2.5	0.2	0.8	68					
8.58		3	b.d.	b.d.	22	0.5	2	b.d.	0.9	71	3	21	17	8	22
10.73	Strongly altered	4	0.2	b.d.	24	0.5	2	0.5	1.0	68	4	20	14	11	19
11.30	Opalinus Clay	6	0.5	b.d.	25	0.5	1.5	1.1	0.9	65					
12.10		5	1.0	b.d.	22	0.5	1	0.3	1.0	70		22	15	11	22
14.33		8	1.5	2	19	b.d.	2	1.0	1.0	65					
15.28	Moderately altered	5	1.0	2.5	23	0.5	2	0.4	1.0	65	2	19	12	10	22
15.94	Opalinus Clay	7	1.5	1.5	25	0.5	3	0.5	1.0	60					
16.75		9	1.0	1.5	28	0.5	3	0.8	0.9	56					
18.16	Decompacted Opalinus Clay	8	1.5	1	21	1	2.5	1.1	1.0	63					
19.62		9	0.5	4.5	23	0.5	2	1.6	0.9	58					
20.09		7	1.5	1	26	0.5	3	0.6	1.0	60					
22.61		8	1.5	2.5	22	1	3	b.d.	1.1	61					
24.52		8	0.5	3.5	22	1	2	2.7	1.0	59	b.d.	17	12	8	23
29.02		9	1.5	1	28	0.5	4	1.1	0.9	54					
33.15		9	1.5	3	24	1	1	b.d.	0.9	59					
33.65		8	b.d.	5.5	30	1.5	2.5	0.3	0.8	51					
38.20		11	1.5	0.5	33	1	5	0.8	0.6	46					
42.88		8	1.0	0.5	40	1	5	0.3	0.7	44					
47.58		9	1.5	1	37	b.d.	3	0.6	0.7	47					
50.13		7	b.d.	3.5	35	1.5	2.5	0.7	0.8	49					
54.98		12	1.5	1.5	42	0.5	3.5	b.d.	0.6	39					
58.33		6	1.5	1	32	1.5	4	0.3	0.7	53					
60.78		6	0.5	1	31	1.5	2	0.5	0.9	56	b.d.				
61.67		7	1.5	0.5	27	1	3.5	0.5	0.9	58					
61.82	Unweathered	5	2.5	5.5	20	b.d.	2.5	1.4	0.9	63					
70.43	Opalinus Clay	3	1.0	b.d.	13	b.d.	2	1.6	1.0	78					

Dolomite/ankerite, siderite, albite and K-feldspars are rounded to 0.5 wt%. b.d. = below detection; empty field = no data. Goethite contents are based on 57Mössbauer spectrometry and the Fe contents of the total rock (see below).

strongly altered zone). Reduced calcite and dolomite contents are also limited to this zone. It is thus evident that there is no single reaction front as considered by Bao et al. (2017) for a reactive-transport model for weathering of the Opalinus Clay in southern Germany. In the moderately altered zone, the effects of weathering reactions on mineralogy are subordinate in quantitative terms.

3.3. Fe-bearing phases identified by X-ray diffraction

Apart from the phases documented above, a broad, small XRD peak at d = 4.18 Å can be identified in the clay-mineral fraction (but not in the bulk-rock powders) of the uppermost 4 studied samples (7.83, 8.58, 10.73, 12.10 m) and represents goethite. Given the brown colour of these samples, a substantial amount of Fe-hydroxides would be expected. The fact that the peak is so small is likely due to a limited grain size and crystallinity. Therefore, a proper quantification cannot be performed on the basis of X-ray diffraction alone.

Total iron contents in the rock were quantified by X-ray fluorescence and are listed in Table 3. No systematic differences can be identified between altered and unweathered Opalinus Clay, suggesting that the mobility of Fe in the weathered zone is limited. Table 3 also lists the Fe inventories in Fe-bearing minerals that were quantified by XRD. Siderite and pyrite were assumed to have stoichiometric compositions, whereas dolomite/ankerite was assumed to have a composition $Ca_{0.59}Mg_{0.34}Fe_{0.07}(CO_3)$, based on chemical data compiled in Pekala et al. (2018). In the unaltered Opalinus Clay, about 35–78% of total Fe is hosted in minerals other than siderite, dolomite/ankerite and pyrite. The additional Fe carriers are clay minerals, in particular chlorite. In the strongly altered zone, the fraction of Fe hosted by siderite, dolomite/ankerite and pyrite amounts to <5%, reflecting the fact that these minerals were dissolved to a large degree in this zone.

3.4. Fe-bearing phases identified by ^{57}Fe Mössbauer spectrometry

^{57}Fe Mössbauer spectrometry can be a useful tool for the identification and quantification of Fe-bearing minerals, even though there are limitations related to the chemical and mineralogical complexity of rocks. The combination with other data, such as mineralogical and chemical rock composition, leads to a better constrained quantification of Fe minerals by fitting the acquired spectra, as well as the estimation of Fe^{2+}/Fe^{3+} ratios. The attribution of components of the acquired spectra to mineral phases is given in Table S1. The Mössbauer spectra at room temperature and at 77 K are documented in Fig. S2. The resulting contents of Fe^{2+} and Fe^{3+} phases are listed in Table 4 and shown graphically as a function of depth in Fig. 4. The following observations can be made:

- The spectra of samples at 10.73 m and deeper present two distinct contributions attributed to Fe^{2+}-bearing species. The contribution with a smaller quadrupolar splitting has parameters consistent with those of siderite (Stevens et al., 2005). However, it cannot be excluded that it partially originates from structural Fe^{2+} in clay minerals. In Table 4, the whole signal is attributed to siderite, i.e. the listed data represent maximum values.
- Magnetic species are only identified in samples from the strongly and moderately altered zones at 77 K and are attributed to mid-sized goethite (5–25 nm). Goethite is the dominating Fe carrier in these samples but drops below detection in the unweathered rock. Combining the Mössbauer data (Table 4) and the total Fe contents in the rock (Table 3) yields goethite contents of 3–4 wt% in the strongly altered and about 1–2 wt% in the moderately altered zone.
- In the unweathered rock, paramagnetic high-spin Fe^{3+} species, most probably clay minerals, are the main carriers of Fe^{3+}. In the uppermost part of the strongly altered zone, the contents in paramagnetic high-spin Fe^{3+} increase. This Fe^{3+} is most likely attributed to oxidised chlorite, as suggested by X-ray diffraction data, with possible contributions of nano-goethite (~ < 5 nm).
- Clay minerals are the main carriers of Fe^{2+} in the unweathered rock. In the strongly altered zone, Fe^{2+} related to clay minerals decreases substantially, likely due to the oxidation of chlorite.
- The contents of Fe^{2+} related to carbonates (mostly siderite) and pyrite are substantially lower in the strongly altered zone, which is due to the observed mineral dissolution.
- Fe^{2+} contents in pyrite and in carbonates obtained from X-ray diffraction and assumed phase compositions on the one hand and from ^{57}Fe Mössbauer spectrometry on the other hand yield similar trends and, given the methodological differences, can be considered to be consistent.

The reduction level (Fe^{2+}/Fe_{tot}) was derived from the Mössbauer data and, independently, by a wet-chemistry approach (phenanthroline method, see Supplementary materials; both data sets are listed in Table 4 and shown in Fig. 4). Both methods agree within 10% and indicate a high reduction level of 83–95% in the unweathered rock, whereas a progressive decrease to 18% in the shallowest sample is identified within the altered zone. Note that no ferrihydrite has been identified, whereas Bao et al. (2017) selected this phase to represent the main carrier of Fe^{3+} in their model calculations.

4. Results and discussion of pore-water studies

The composition of pore waters was investigated by aqueous extraction, squeezing tests (major-ion composition) and the diffusive exchange method (stable water isotopes).

4.1. Squeezing data

Chemical compositions of squeezed waters are listed in Table 5. Total mineralisation is around 1 g/L in the altered and decompacted zones. Then it increases rapidly until reaching values of 11–13 g/L in sample 37.30 m and deeper. The ionic strength of the Opalinus Clay samples below 40 m is 0.24–0.26, which is comparable with that obtained at other locations in the region (range 0.1–0.4, Wersin et al., 2020, 2022). Also, cation concentrations and ratios are within the ranges of the regional data. The chemical water type evolves from Ca-SO_4-HCO_3 in the strongly altered zone to Na-SO_4-Cl in the decompacted zone and the fresh rock below. This is a remarkable contrast to regional data for the

Table 3
Distribution of Fe in different minerals based on chemical (X-ray fluorescence) and mineralogical (X-ray diffraction) data.

Depth [m]	Unit	Fe_{tot} in rock based on XRF [g/kg]	Fe in pyrite [g/kg]	Fe in siderite [g/kg]	Fe in dolomite/ankerite [g/kg]	Fe in pyrite [% of Fe_{tot}]	Fe in siderite [% of Fe_{tot}]	Fe in dol/ank [% of Fe_{tot}]	Fe in other phases [% of Fe_{tot}]
7.83	Strongly altered	47.70	0.6	b.d.	b.d.	1.2	b.d.	b.d.	98.8
8.58		39.31	0.1	b.d.	b.d.	0.3	b.d.	b.d.	99.7
10.73		47.77	2.1	b.d.	0.1	4.5	b.d.	0.2	95.3
12.10	Moderately altered	41.62	1.3	b.d.	0.3	3.1	b.d.	0.8	96.1
15.28		39.52	1.9	12.0	0.4	4.7	30.3	1.0	64.1
24.52		48.26	12.4	17.0	0.1	25.6	35.1	0.3	39.0
33.65	Unweathered	44.20	1.2	27.4	b.d.	2.7	62.0	b.d.	35.3
60.78		34.27	2.6	4.7	0.1	7.5	13.7	0.4	78.4

Table 4
Distribution of Fe for different minerals based on ^{57}Fe Mössbauer spectrometry. Data based on spectra at 77 K, except for carbonates.

Depth [m]	Unit	Fe^{3+} in paramag. high-spin-Fe^{3+} phases (clay minerals, ±nano-goethite) [% of Fe_{tot}]	Fe^{3+} in goethite 5–25 nm [% of Fe_{tot}]	Fe^{2+} in pyrite [% of Fe_{tot}]	Fe^{2+} in high-spin- Fe^{2+} phases (sum clay minerals + carbonates) [% of Fe_{tot}]	Fe^{2+} in siderite (maximum) [% of Fe_{tot}]	Total Fe^{2+} [% of Fe_{tot}]	Total Fe^{2+} by phenanthroline method [% of Fe_{tot}]
7.83	Strongly altered	25	57	<1	18	<1	18	19
8.58		31	45	<1	24	<1	24	29
10.73		16	54	≤5	25	2	30	36
15.28	Moderately altered	16	25	≤4	55	26	59	61
24.52*	Unweathered	15	<1	≤16	69	28	85	83
60.78		14	<1	≤5	81	26	86	95

* In this sample, multiple fits are possible because one of the components attributed to HS-Fe^{3+} has hyperfine parameters very close to those of pyrite. Therefore, the given contents of pyrite and paramagnetic HS-Fe^{3+} species are uncertain.

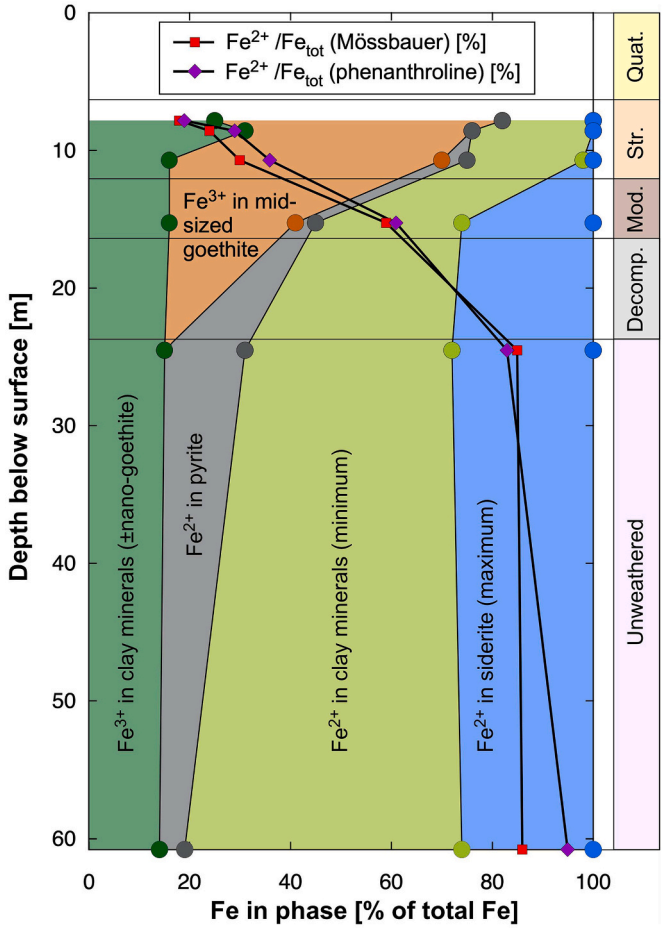

Fig. 4. Depth profile of Fe-bearing minerals based on ^{57}Fe Mössbauer spectrometry. Black lines show the reduction level (Fe^{2+}/Fe_{tot}) based on two different methods.

Opalinus Clay, according to which pore waters are mostly of the Na—Cl type (borehole and squeezed waters in the Opalinus Clay from the Mont Terri Underground Research Laboratory, 46 km WSW of Lausen, Pearson et al., 2003; 2011; Wersin et al., 2006; 2010; Gimmi et al., 2014; Vinsot et al., 2008; Vinsot et al., 2014; Fernández et al., 2014; Mazurek et al., 2017b; Bleyen et al., 2017; squeezed waters from borehole Bülach-1, 58 km ENE, Mazurek et al., 2021; and squeezed waters from borehole Schlattingen-1, 79 km NE, Mazurek et al., 2015).

Mineral saturation indices for squeezed waters were calculated using PHREEQC Version 3 (Parkhurst and Appelo, 2013) and the Thermochimie database (Giffaut et al., 2014). Methodological uncertainties exist regarding carbonate minerals (enhanced solubility at high pressures during squeezing, potential outgassing during the experiments; Mazurek et al., 2015, 2021), so data are only given for sulphate minerals in Table 5. In the unweathered Opalinus Clay, pore waters are close to saturation with respect to gypsum and celestite (except for the shallowest samples), whereas undersaturation with respect to all sulphate minerals is identified in the weathered zone. According to regional data, deep pore waters in the Opalinus Clay are saturated with respect to celestite but typically undersaturated with respect to gypsum and anhydrite.

As shown in Fig. 5, pore water in the unweathered Opalinus Clay at Lausen has distinctly high SO_4^{2-} and low Cl^- contents, whereas the SO_4^{2-}/Cl^- ratio in regional boreholes is close to or slightly above the value of modern sea water. One potential source of SO_4^{2-} are the underlying Triassic rocks that contain anhydrite. However, anhydrite-bearing beds underlie the Jurassic at all other sites as well, yet SO_4^{2-} contents in the Opalinus Clay remain distinctly lower. Note that the regional data refer to depths >250 m, so the question arises whether the source of SO_4^{2-} at Lausen could be related to the proximity of the surface, i.e. to surficial oxidation of pyrite. SO_4^{2-} could have accumulated in gypsum, followed by dissolution during more humid periods and SO_4^{2-} transport to depth.

4.2. Data from aqueous extraction

Selected results of aqueous-extraction tests are listed in Table 6. Cl^- concentrations in extracts were recalculated to concentrations in free pore water according to

$$Cl^-_{\text{free pore water}} = \frac{Cl^-_{\text{aq.extract}}}{WC_{\text{dry}}\ S/_L\ \alpha}$$

with WC_{dry} = gravimetric water content relative to dry mass
S/L = solid/liquid ratio
α = anion-accessible porosity fraction.

The factor α considers anion exclusion adjacent to negatively charged clay surfaces (see, e.g., Appelo, 1977, Israelachvili, 1991). It can be obtained by dividing the Cl^- concentration in the total pore water (obtained by aqueous extraction) by that in the free pore water (obtained by squeezing). Further methodological details are documented in Mazurek et al. (2015). For the unweathered Opalinus Clay at Lausen, an average value of 0.58 was obtained for α and was used for the recalculation of Cl^- data from aqueous-extraction tests to concentrations in free pore water. This value is close to the value of 0.54 obtained by Pearson et al. (2003) for the Opalinus Clay in the Mont Terri Underground Research Laboratory. The calculated Cl^- contents in free pore water are also listed in Table 6, and a depth profile is shown in Fig. 6, together with data from squeezing. At shallow levels to a depth of 20 m, Cl^- contents are low. This zone contains a fracture network that may have facilitated circulation of surface waters. Between 20 and about 40 m, a sharp increase of Cl^- concentration is identified, followed by near-constant values of about 3 g/L below 40 m. The hypothesis that this

Table 5
Chemical composition of squeezed waters and mineral saturation indices (SD).

Depth [m]	Unit	Squeezing pressure [MPa]	Mass squeezed [g]	Na^+ [mg/L]	K^+ [mg/L]	Ca^{2+} [mg/L]	Mg^{2+} [mg/L]	Sr^{2+} [mg/L]	Cl^- [mg/L]	Br^- [mg/L]	SO_4^{2-} [mg/L]	TIC as HCO_3^- [mg/L]	TOC [mg/L]	TDS [g/L]	pH	SI gypsum	SI anhydrite	SI celestite
10.88	Str. alt. OPA	20	5.81	65.2	14.8	200	35.5	0.96	41.4	<0.16	548	225	18.2	1.13	7.99	−0.67	−0.84	−1.31
15.05	Mod. alt. OPA	20	4.13	82.1	8.32	43.7	17.4	0.83	30.1	<0.16	94.9	335	15.6	0.61	8.52	−1.85	−2.02	−1.88
19.05	Decomp. OPA	50	3.61	175	13.0	58.1	35.9	3.87	38.9	<0.8	402	283	28.1	1.01	8.48	−1.26	−1.43	−0.76
24.93	Unweathered	50	2.06	1167	37.0	179	103	6.30	739	<0.8	2270	178	82.2	4.68	8.22	−0.49	−0.66	−0.27
29.28	Opalinus Clay	100	3.72	1880	44.3	355	195	9.50	1269	1.50	4042	144	64.8	7.94	8.06	−0.14	−0.31	−0.04
34.13		100	2.28	2408	51.8	417	232	10.7	1936	2.15	4649	134	69.8	9.84	7.88	−0.07	−0.24	0.01
37.30		100	0.97	2923	59.0	447	230	6.95	2360	2.65	4634	164	137	10.83	8.12	−0.07	−0.24	−0.21
41.68		150	1.36	3090	59.6	536	232	10.2	2566	2.90	5261	172	88.9	11.93	8.41	0.02	−0.14	−0.02
49.75		100	0.48	3224	70.9	454	242	6.25	3180	3.80	4387			11.57	8.11	−0.09	−0.26	−0.29
71.08		100	1.77	3047	54.3	453	264	7.85	3242	4.10	4221	168	118	11.46	7.88	−0.11	−0.27	−0.20
80.47	Staffelegg Fm.	300	1.29	3313	57.5	548	299	10.3	3428	4.55	5033	161	83.8	12.85	8.03	0.00	−0.16	−0.06
113.79	Klettgau Fm.	300	1.30	3469	59.6	475	232	8.00	3441	5.00	4905	159	69.4	12.75	8.04	−0.06	−0.23	−0.16

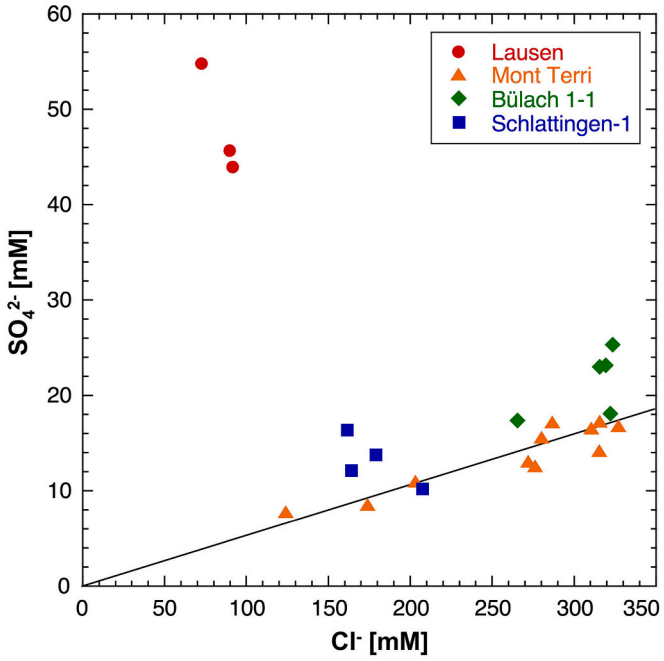

Fig. 5. Cl^- and SO_4^{2-} contents of squeezed pore waters in the Opalinus Clay from Lausen (only samples from depths >40 m) in comparison with regional data (for references see text). Line indicates the SO_4^{2-}/Cl^- ratio in modern sea water (0.052).

profile can be explained by out-diffusion towards the surface is explored below.

Table 6 also lists the concentrations of NO_3^- and NH_4^+ in aqueous extracts. The ratio NH_4^+/NO_3^- evolves from 0.27 in the shallowest sample to 2.5–5.5 in the unweathered underlying rock. Until a depth of about 17 m, it is clearly lower than in the unweathered rock. It is concluded that NH_4^+ is affected by oxidation to a depth comparable to that of the occurrence of goethite and lower Fe^{2+}/Fe_{tot} ratio as obtained from Mössbauer spectrometry.

4.3. Stable water isotopes

The depth profiles of $\delta^{18}O$ and δ^2H of pore water are listed in Table 6 and shown in Fig. 7. Both profiles indicate δ values increasing with depth until about 60–80 m, below which depth they remain largely constant. However, within the uppermost 35 m, the trend is complicated by local disturbances of both $\delta^{18}O$ and δ^2H. Thus, the profiles of Cl^- and water isotopes are distinctly different and will be further explored below.

4.4. Ground waters, redox state and implications for the water table

Three ground-water samples were taken in the weathered zone (Vogt et al., 2017). All of them are overpressured, with an equivalent head ≥10 m above the hydrostat. This can be explained by topography, as the site is located in a valley position close to a hill (Fig. 1). Together with the consistency between porosities obtained from water content (representing the water-filled pore space) and from densities (representing the total pore space; Table 2), this indicates full saturation, i.e. the ground-water table is located in the overlying, 6 m thick Quaternary cover. Two of the ground-water samples, covering the depth interval 8.3–18.4 m, are only weakly contaminated by drilling fluid (≤0.2% based on uranine; Vogt et al., 2017). Remarkably, O_2 contents are only 0.2–0.7 mg/L (Vogt et al., 2017), compared with about 8 mg/L in air-equilibrated water, and even these low contents are likely the result of contamination. This is also suggested by the measurable Fe^{2+} and Mn^{2+}

Table 6
Cl^-, NH_4^+ and NO_3^- concentrations in aqueous extracts and isotopic composition of pore water obtained by the diffusive exchange technique. Further, calculated Cl^- contents in free pore water are given. n.q. = not quantified.

Depth [m b. g.]	Formation	*S/L*	Cl^- in aqueous extract [mg/L]	Cl^- in free pore water [mg/L]	NH_4^+ in aqueous extract [mg/L]	NO_3^- in aqueous extract [mg/L]	NH_4^+/NO_3^- (mass units)	$\delta^{18}O$ [‰ V-SMOW]	$\delta^{18}O$ error [‰ V-SMOW]	δ^2H [‰ V-SMOW]	δ^2H error [‰ V-SMOW]	Deuterium excess [‰]
7.83	Strongly altered Opalinus Clay	0.699	1.45	16.2	0.15	0.56	0.27	−8.58	0.13	−63.6	1.3	5.0
8.23		0.726	1.88	24.1	0.13	0.43	0.30	−8.54	0.13	−63.6	1.3	4.7
8.58		0.758	2.15	26.5	0.13	0.27	0.48	−8.52	0.13	−64.0	1.3	4.2
10.73		0.746	2.44	34.3	0.19	0.23	0.80	−8.37	0.13	−63.8	1.3	3.2
11.30	Moderately altered Opalinus Clay	0.750	2.22	31.8	0.15	0.31	0.49	−8.35	0.14	−63.6	1.3	3.2
12.10		0.782	2.03	31.8	0.31	0.21	1.49	−8.21	0.14	−63.2	1.3	2.5
15.28		0.815	1.62	29.8	0.60	0.39	1.56	−8.07	0.15	−61.3	1.4	3.3
15.94		0.824	1.42	28.1	0.38	0.41	0.94	−7.88	0.15	−60.4	1.4	2.6
16.75	Decompacted Opalinus Clay	0.837	1.03	22.3	0.50	0.64	0.78	−7.78	0.14	−59.8	1.4	2.4
19.62		0.857	1.92	46.5	<1	0.05		−7.80	0.15	−59.7	1.5	2.7
20.09		0.861	1.94	47.1	<1	0.54		−7.64	0.16	−59.8	1.5	1.3
24.52	Unweathered Opalinus Clay	0.906	19.9	510	1.50	0.61	2.46	−8.35	0.16	−63.2	1.5	3.6
29.02		0.883	36.4	1067	1.54	0.60	2.57	−8.74	0.16	−65.2	1.5	4.7
33.65		0.916	56.1	1686	n.q.	0.30		−8.67	0.17	−63.2	1.6	6.2
42.88		0.914	81.6	2771	<1	0.58		−7.89	0.19	−56.2	1.8	6.9
47.58		0.896	85.3	2847	1.70	0.65	2.62	−7.80	0.17	−54.1	1.7	8.3
50.13		0.891	85.7	2873	n.q.	0.24		−7.56	0.18	−52.2	1.8	8.3
54.98		0.905	86.5	3071	<1	0.56		−7.79	0.18	−52.9	1.8	9.4
60.78		0.888	88.7	2895	n.q.	0.32		−7.47	0.18	−49.4	1.9	10.4
77.81		0.923	73.1	3183	2.05	0.37	5.54	−6.53	0.22	−45.7	2.2	6.5
82.87	Staffelegg Fm.	0.908	87.1	3023	n.q.	0.61		−7.33	0.17	−47.2	1.8	11.4
96.98		0.909	83.0	3057	2.09	0.68	3.07	−7.32	0.18	−46.3	1.9	12.3
113.55	Klettgau Fm.	0.889	103	2909	n.q.	0.37		−7.63	0.17	−46.2	1.7	14.8
132.12		0.914	85.7	3452	<1	0.54		−7.08	0.21	−43.9	2.2	12.7

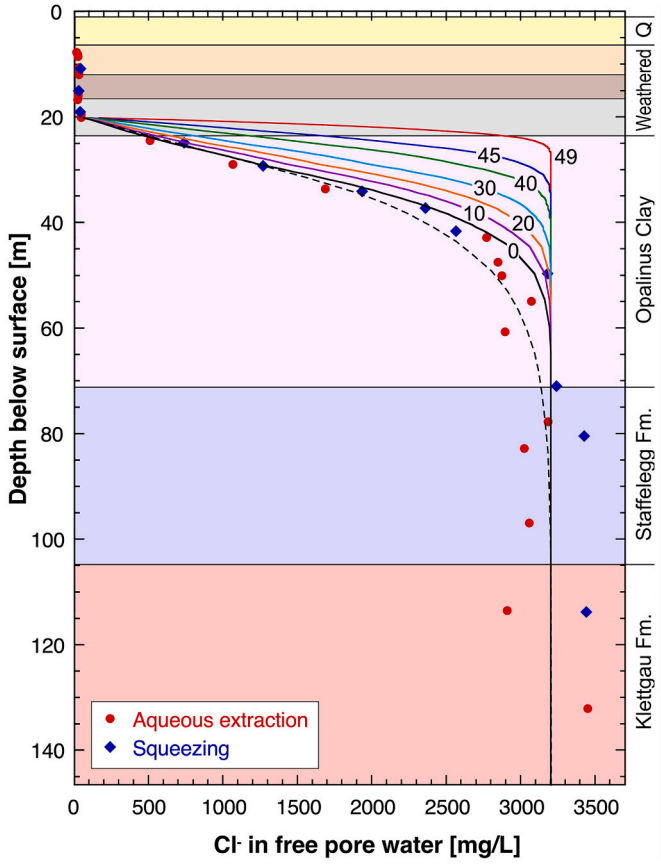

Fig. 6. Depth profile of Cl^- in free pore water, and model calculations reproducing the observed Cl^- profile by pure diffusion (solid lines, process starting at 50 ka) or combined upward advection and diffusion (stippled line shows the steady-state situation). Numbers indicate geological ages in ka.

contents in both waters, indicative of reducing conditions. It is concluded that even at the shallowest levels, redox is efficiently buffered by the rock, and oxygen is consumed. As shown above (e.g. Table 2), organic matter and pyrite have reduced contents in the uppermost 2 m of the Opalinus Clay but are still present and available to consume dissolved O_2. Thus, it appears unlikely that the current waters would be capable of producing the massive oxidation identified in the weathered zone. Bao et al. (2017) concluded in a modelling study that the most important parameter controlling the progress of reactions of chemical weathering is the supply of oxygen via gas diffusion in the partially saturated uppermost part of the formation. For an exposure time of 10 kyr, they predicted a thickness of about 2 m for the weathered zone in the Opalinus Clay of southern Germany. In Lausen, the weathered zone is much thicker, even though oxygen transport throughout the Holocene is considered to have taken place via aqueous diffusion in the saturated pore space, a process that is much slower in comparison to gas diffusion. It is concluded that the weathered zone must have developed over longer periods of time than just the Holocene. Most probably, the water table was lower in the past, leading to unsaturated conditions in the weathered zone. This may have been the case during arid climates of the Pleistocene, given the fact that the Lausen site was not ice-covered since about 500 ka. This conclusion is relevant for the modelling calculations that follow in the next section.

5. Modelling of pore-water tracers

5.1. Modelling strategy

Calculations considering transport of the conservative tracers Cl^-, $\delta^{18}O$ and δ^2H across the water-saturated pore space were performed using FLOTRAN (Lichtner, 2004; see Supplementary materials S2 for details). Diffusion and, in some cases, advection were considered as transport processes. Given the fact that diffusion coefficients were not measured for the Lausen core, they were estimated from the free-water coefficients of Li and Gregory (1974) and measured porosities, using the modified Archie's law of Van Loon and Mibus (2015). In the present case, the modification is of minor relevance (it becomes important for

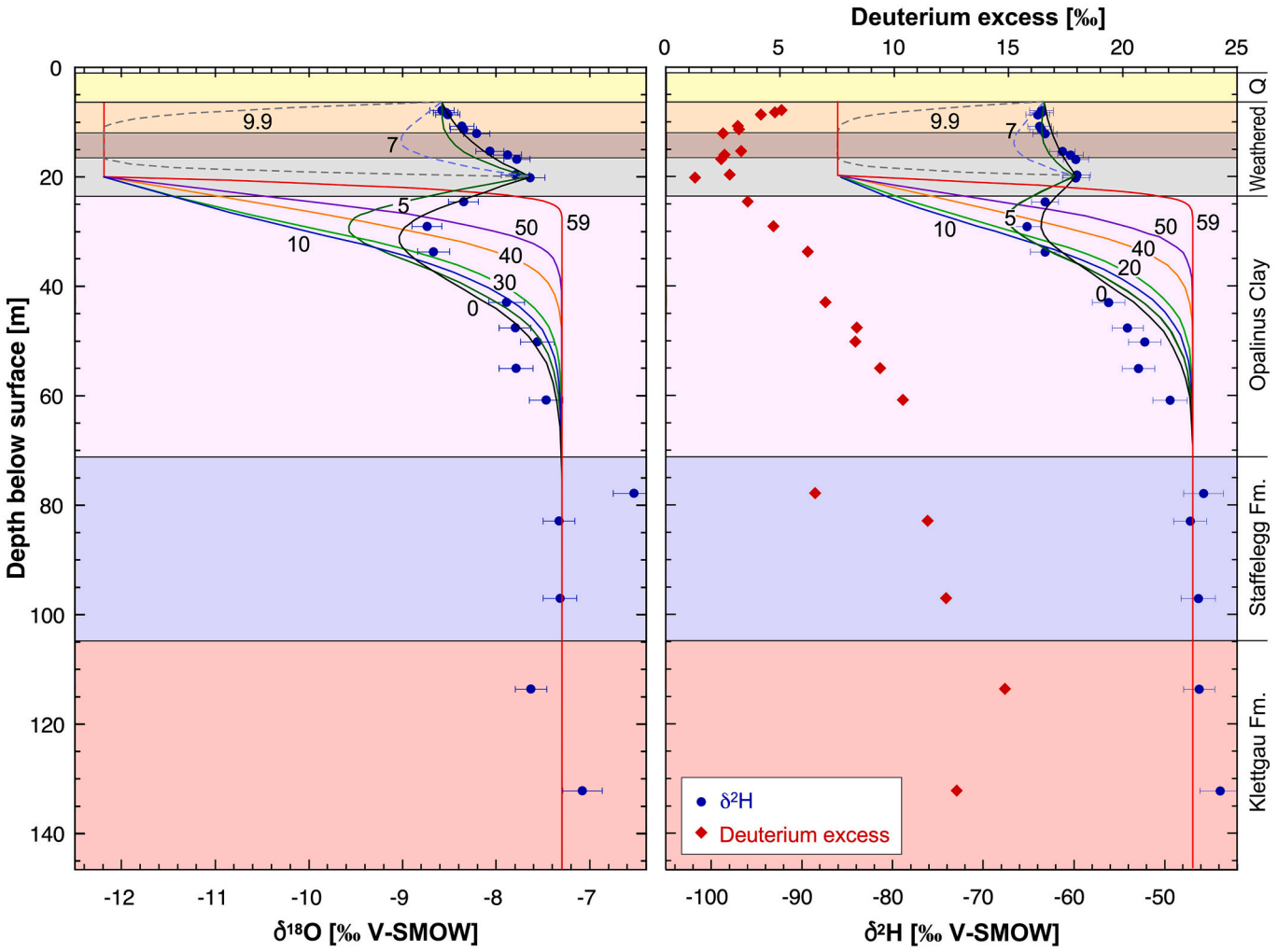

Fig. 7. Depth profile of $\delta^{18}O$, $\delta^{2}H$ and deuterium excess in pore water based on diffusive-exchange experiments, and modelled distributions of $\delta^{18}O$ and $\delta^{2}H$ according to the scenario described in Table 8. Numbers indicate geological ages in ka.

small porosities) and is close to a simple Archie's equation with an exponent of 2.4. Due to the wide range of porosities encountered in the Lausen profile (Table 1, Fig. 3), a number of layers were defined, and the pertinent data are listed in Table 7. Diffusion coefficients obtained for the deeper parts of the profile (unaffected by weathering and decompaction) compare favourably with experimental data obtained for the Opalinus Clay at the Mont Terri Underground Laboratory by Van Loon and Soler (2003) and Van Loon et al. (2005a, 2005b), as shown in Table 7.

The current temperature in the Lausen borehole is around 13 °C. Diffusion coefficients were corrected for the temperature effect using the experimental approach of Van Loon et al. (2005a) for the Opalinus Clay. Given the fact that the modelled periods extend back into the Pleistocene, time-dependent diffusion coefficients were used, and assumptions

Table 7
Averages of measured porosities and calculated effective and pore-diffusion coefficients for the Lausen core. Experimental Mont Terri data from Van Loon and Soler (2003) and Van Loon et al. (2005a, 2005b) are shown for comparison. All data refer to the direction normal to bedding and a temperature of 25 °C.

Depth [m]	Total porosity [−]	Cl^--accessible porosity [−]	D_e (HTO) [m^2/s]	D_e (Cl^-) [m^2/s]	D_p (HTO) [m^2/s]	D_p (Cl^-) [m^2/s]
6.2–7.5	0.390	0.226	2.3E-10	5.9E-11	5.9E-10	2.6E-10
7.5–9.0	0.359	0.208	1.9E-10	4.8E-11	5.2E-10	2.3E-10
9.0–10.3	0.330	0.192	1.5E-10	4.0E-11	4.7E-10	2.1E-10
10.3–11.7	0.305	0.177	1.3E-10	3.3E-11	4.2E-10	1.9E-10
11.7–13.3	0.280	0.163	1.0E-10	2.7E-11	3.7E-10	1.7E-10
13.3–15.0	0.257	0.149	8.5E-11	2.2E-11	3.3E-10	1.5E-10
15.0–16.5	0.237	0.137	7.0E-11	1.8E-11	3.0E-10	1.3E-10
16.5–18.3	0.218	0.127	5.8E-11	1.5E-11	2.7E-10	1.2E-10
18.3–20.0	0.201	0.116	4.8E-11	1.3E-11	2.4E-10	1.1E-10
20.0–22.5	0.184	0.107	3.9E-11	1.0E-11	2.1E-10	9.8E-11
22.5–25.0	0.170	0.099	3.2E-11	8.7E-12	1.9E-10	8.8E-11
25.0–28.5	0.156	0.091	2.7E-11	7.2E-12	1.7E-10	7.9E-11
28.5–42.0	0.140	0.081	2.1E-11	5.6E-12	1.5E-10	6.9E-11
42.0–	0.135	0.078	1.9E-11	5.2E-12	1.4E-10	6.7E-11
Mont Terri	0.10–0.17	0.058–0.077	1.2–1.5E-11	4.1–5.5E-12	0.8–1.6E-10	5.5–9.7E-11

had to be made regarding the evolution of temperature over the period of interest. According to Fauquette et al. (1999) and Delisle et al. (2003), mean ground temperatures in the period 10–50 ka were about 10 °C below current temperature. For the correction of the diffusion coefficients, the ground temperatures were assumed to be identical to surface temperatures, which is not strictly the case but of limited quantitative importance.

5.2. Cl^- profile

The curved shape of the Cl^- profile suggests a diffusion-dominated system below a depth of 20 m, and this scenario was quantified by model calculations. Assuming an initial Cl^- concentration of 3.2 g/L (the mean concentration observed below 40 m depth), the data can be reproduced quite well, and an evolution since about 50 ka can be obtained (Fig. 6). However, the assumption of a constant initial Cl^- concentration at 20 m depth and deeper cannot be justified independently and so remains uncertain.

In an alternative model scenario, the Cl^- profile was considered to represent a steady-state situation with out-diffusion towards the surface and an upward-directed advective component. A good fit to the data can be obtained for a Darcy velocity of 1×10^{-5} m/yr ($=3.2 \times 10^{-13}$ m/s), and steady state is closely approached after an evolution time of about 300 kyr (also shown in Fig. 6). Considering a hydraulic conductivity of 3×10^{-13} to 5×10^{-13} m/s parallel to bedding (measured value for the lower part of the Opalinus Clay, Vogt et al., 2017) and an anisotropy factor of 5 (Yu et al., 2017), such a Darcy velocity requires an upward-directed hydraulic gradient of about 3–5 over the whole model period, which is considered to be unlikely because natural gradients are typically much smaller (Neuzil, 2019). Therefore, the steady-state model scenario is considered less realistic, leading to the conclusion that the Cl^- profile is transient and evolved over the last few tens of thousands of years.

5.3. Profiles of water isotopes

The deeper penetration of the surficial signal to about 60–80 m in comparison with Cl^- (Fig. 6, Fig. 7) is consistent with the higher diffusion coefficient for H_2O. Within the uppermost 35 m, the trend is complicated by local disturbances of both $\delta^{18}O$ and δ^2H, a feature not seen for Cl^-. A local maximum is identified at about 20 m, close to the base of the weathered zone, and a minimum at 30 m. Both are remarkably sharp and so cannot be explained by a temporally variable upper boundary condition. In particular, the trends from both sides towards the maximum at 20 m are near-linear, best explained by steady-state diffusion. Given the steep gradients of both isotope ratios in this zone, the disturbance must be young because otherwise diffusion would have obliterated it. Further, deuterium excess decreases with depth in the weathered zone and reaches a distinct minimum at 20 m (Table 6, Fig. 7), with a position markedly below the local meteoric water line in a plot of $\delta^{18}O$ vs. δ^2H. Thus, the shapes of the $\delta^{18}O$ and δ^2H profiles as well as the deviation of the data from the meteoric water line (i.e. deuterium excess) suggest the presence of a hydraulic boundary at this depth, most likely a fracture with flowing water. This boundary also coincides with the base of the zone of low water salinity (Fig. 6). Indeed, a prominent fracture steeply dipping to NNE was identified in the core and is illustrated in Fig. 2b.

The δ values at 20 m depth are higher than those of recent local recharge. Together with the negative excursion of deuterium excess, this water could be explained as due to partial evaporation in the source region. In a study targeted at the Tégulines Clay in France, Lerouge et al. (2018) also suggested evaporation as a potential process to explain ^{18}O- and ^2H-enriched pore waters in the studied weathering profile. In contrast, water-rock interactions within the weathered zone cannot explain the observed deviation from the meteoric water line. Carbonate dissolution is quantitatively insufficient to account for the shift, and precipitation of goethite would shift the coexisting water above the meteoric water line (using the fractionation factors of Yapp et al. 1987).

The interpretation of the near-linear trends of both isotope ratios in the weathered zone down to 20 m as diffusion profiles is in apparent contradiction to the fact that fractures were observed in this zone and some of them show oxidised rims in an otherwise reduced matrix, which clearly indicates that fracture flow occurred (example in Fig. 2a). A solution to this conundrum is offered by the variation of the water table as postulated above based on independent arguments. Partial saturation during arid periods in the Pleistocene resulted in shrinkage of the clay, leading to enhanced apertures and flow of oxidising waters in fractures. Duprat-Oualid (2019) characterised climate conditions based on pollen studies from a local lake sediment profile and concluded that steppe vegetation dominated in the studied period (45–15 ka). Further, the linkage of biological and climate data yielded estimates of precipitation rates, which were indeed well below current values. With the onset of the Holocene, climate became more humid and lifted the water table to the current level. The consequence of full resaturation within the uppermost 20 m is fracture self-sealing by swelling. The fact that a fracture at 20 m depth remained open might be explained by the more consolidated nature of the rock at this depth when compared to the highly porous, plastic clay at shallower levels (Fig. 3).

In order to estimate the time scales related to the evolution of the observed profiles of $\delta^{18}O$ and δ^2H, model calculations were performed in a similar way as for Cl^-. The main parameters are summarised in Table 8. The modelling period was divided into a Pleistocene and a Holocene scenario. For the Pleistocene, spatially constant initial δ values corresponding to those measured for the deeper parts of the profile were considered. The top of the Pleistocene model was the fracture at 20 m. At the time of activation of this fracture, cold-climate δ values were assumed as upper boundary condition, estimated from regional water-isotope data for ground waters attributed to cold-climate infiltration (Pearson et al., 1991; Waber et al., 2014). The uppermost 20 m were assumed to represent a well-mixed system with constant cold-climate isotopic composition. At the onset of the Holocene at 10 ka, the water-isotopic composition at the boundary at 20 m was shifted to the current value measured in the pore water at 20 m depth, i.e. at the apex of the excursions of $\delta^{18}O$, δ^2H and deuterium excess. In addition, the Holocene evolution of the isotope ratios in the weathered zone above 20 m depth was also tentatively quantified by assuming the present-day values in the uppermost sample at 7.8 m as upper boundary condition.

Model results are illustrated in Fig. 7. The best fit for the evolution of

Table 8
Initial and boundary conditions used for the modelling of the $\delta^{18}O$ and δ^2H profiles.

	Time period 60–10 ka (Pleistocene)	Time period 10–0 ka (Holocene)
Depth interval 6.2–20 m	Well-mixed system, flow in fracture network, possibly at partial saturation, cold-climate isotope values: $\delta^{18}O = -12.2$ ‰, $\delta^2H = -86$ ‰	Diffusion-dominated, saturated system. Top and bottom boundaries approximated by current pore-water values in upper- and lowermost pore-water samples: $\delta^{18}O = -8.58$ ‰, $\delta^2H = -63.6$ ‰ $\delta^{18}O = -7.64$ ‰, $\delta^2H = -59.8$ ‰
Fracture at 20 m	Fracture = upper model boundary with cold-climate isotope signature: $\delta^{18}O = -12.2$ ‰, $\delta^2H = -86$ ‰	Current values at the apex of the excursion of isotope values: $\delta^{18}O = -7.64$ ‰, $\delta^2H = -59.8$ ‰
Depth interval > 20 m	Diffusion-dominated system; initial condition = current δ values at depth: $\delta^{18}O = -7.3$ ‰, $\delta^2H = -47$ ‰	Diffusion-dominated system; initial condition = curved profile resulting from diffusive exchange with the upper boundary over the period 60–10 ka

the deeper part of the profile was obtained for an activation time at 60 ka, which is remarkably similar to the 50 ka obtained for the Cl^- profile. Pleistocene erosion history offers a potential explanation for the modelled evolution times. The regional base level is determined by the Rhine River 8 km to the north (Fig. 1a). Based on studies of regional speleothems, Becker et al. (2020) noted a phase of incision starting in the last interglacial (~110 ka). A minimum base level may have been reached at ~70 ka, at the onset of a cold period with growth of glaciers (marine isotope stage MIS4, Lisiecki and Raymo, 2005). The lower base level may then have propagated towards the Lausen site, explaining the postulated low ground-water level.

Holocene warming and the related shift of the values at the boundary at 20 m at 10 ka also yields good fits to the trends observed at 20–30 m. In the zone above 20 m, steady-state diffusion profiles developed. Note that the slight curvature in the model curves of this interval is due to the depth-dependent porosities and diffusion coefficients used in the model (see Table 7) and not to a transient state.

Thus, the presented scenario reproduces the observations well and is also consistent with the model results obtained for Cl^-. It is concluded that, with the exception of a flowing fracture at 20 m, diffusion is the currently dominating transport mechanism even in the weathered zone of the Opalinus Clay. Geological evidence, such as the presence of oxidised rims along fractures (Fig. 2a) indicates that advection played a role at least during some periods in the past, likely during arid periods in the Pleistocene.

6. Conclusions

Due to long-term surface exposure, the Opalinus Clay at Lausen has experienced significant geochemical, mineralogical and hydraulic changes in the uppermost tens of metres. The main effects are summarised in Fig. 8. It becomes evident that the penetration depth of the different effects varies substantially. Structural changes in the rock following decompaction include a high degree of fracturing and a massive increase of porosity in the uppermost ~30 m. In this interval, hydraulic conductivity is also increased.

From a mineralogical perspective, the complete dissolution of siderite in the strongly altered Opalinus Clay (i.e. to a depth of 12 m below surface) and the precipitation of goethite are the most relevant effects in quantitative terms. In contrast, calcite and dolomite/ankerite are only partially dissolved in this zone. Reduced contents of pyrite and organic matter are only seen in the uppermost 2 m of the Opalinus Clay, but the dissolution remains incomplete even there. Siderite and, to a more limited degree, pyrite are the main sources of Fe for the precipitation of goethite. Alteration becomes weaker in the underlying moderately altered zone (12–16.4 m), below which goethite content becomes negligible and the colour of the rocks turns grey. At all depths, silicate minerals are not affected by weathering, except for some oxidation of chlorite. The reduction level of Fe (Fe^{2+}/Fe_{tot}) in the rock drops from 83-95% in the unweathered rock to <20% at the top of the Opalinus Clay. The reducing conditions identified in the ground waters of the weathered zone suggest that most of the mineralogical alterations did not occur by interaction with the current waters but were triggered by a lower water table during arid periods in the Pleistocene, when oxygen was able to access the formation via gas diffusion.

Based on the profiles of pore-water chemistry and mineralogical data, three evolutionary stages can be distinguished:

1) Unusually high SO_4^{2-} contents and SO_4^{2-}/Cl^- ratios in the

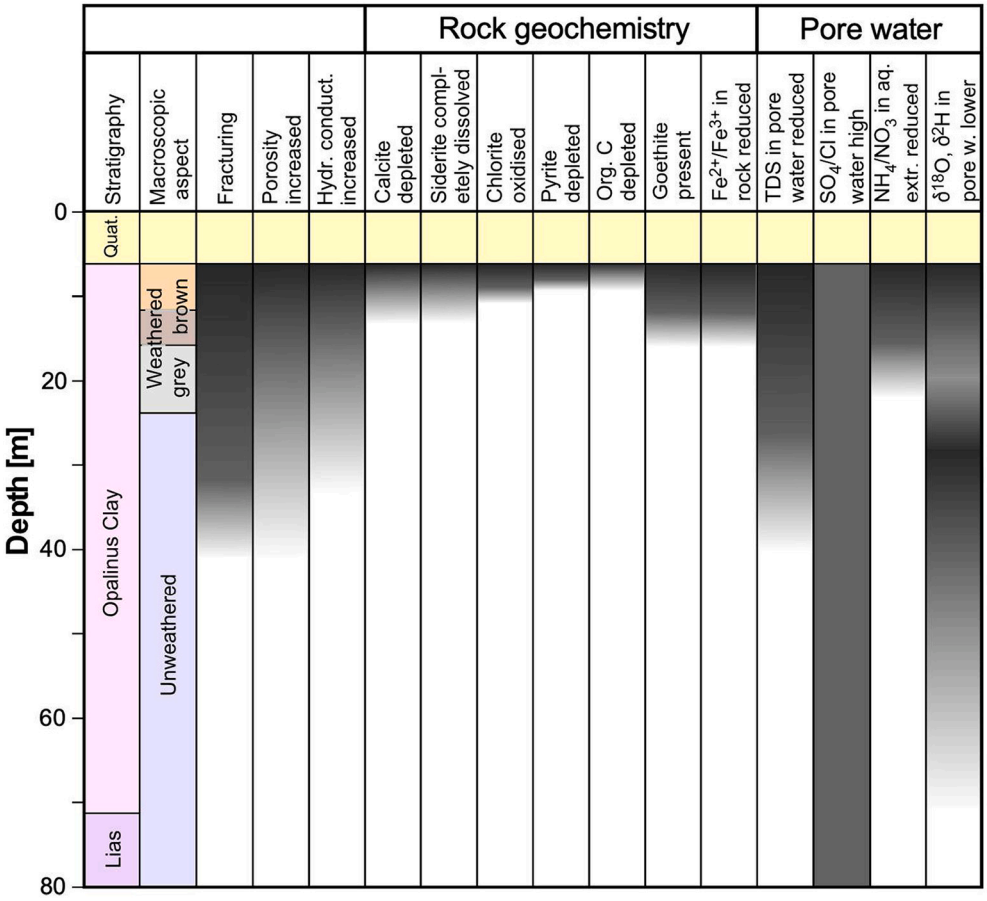

Fig. 8. Synthetic profile summarising the depth penetration of surface effects on rock and pore water. Information on fracturing and hydraulic conductivity is based on Vogt et al. (2017).

unweathered Opalinus Clay indicate input from an external SO_4^{2-} reservoir. This could be the underlying Triassic evaporites or, more likely, SO_4^{2-} from surficial gypsum that precipitated during pyrite oxidation and later dissolved in stages of higher water table. Both the hypothetical accumulation of gypsum and downward transport involve substantial periods of time, so the addition of SO_4^{2-} into the pore water of the unweathered Opalinus Clay is the oldest process in relative terms.

2) Surface effects on water-isotope ratios and Cl^- contents in pore waters reach to depths of 60–80 and 40–50 m, respectively. The modelled ages of the currently observed out-diffusion profiles are in the range 50–60 ka.

3) The complex shapes of the water-isotope profiles at shallow levels are interpreted as an effect of the rise of the water table at the onset of the Holocene, leading to fracture self sealing by swelling and the establishment of a diffusive regime under saturated conditions, even in the strongly weathered zone.

From an applied perspective, it is remarkable that under saturated conditions the depth penetration of rock oxidation is quite limited, which highlights the substantial buffering capacity of the Opalinus Clay against external geochemical disturbances. Also, self sealing of fractures that at earlier times experienced fracture flow (as indicated by oxidised rims) leads to the establishment of a diffusive system even at shallow depth.

Credit author statement

Martin Mazurek: Conceptualisation, methodology, investigation, modelling, writing, visualisation.
Paul Wersin: Investigation, modelling, reviewing.
Jebril Hadi: Investigation, reviewing.
Jean-Marc Grenèche: Investigation, reviewing.
Nouvarat Prinpreecha: Investigation, modelling.
Daniel Traber: Reviewing.

Declaration of Competing Interest

The authors declare that they have no known competing financial interests or personal relationships that could have appeared to influence the work reported in this paper.

Data availability

Data will be made available on request.

Acknowledgements

The authors are grateful for financial support by Nagra. Rock squeezing was performed at CRIEPI (Japan) under the supervision of T. Oyama. Several interesting discussions with T. Gimmi (Uni. Bern and Paul Scherrer Institut) and M. Schnellmann (Nagra) are acknowledged. Two anonymous reviewers provided useful comments that helped to improve the manuscript.

Appendix A. Supplementary data

Supplementary data to this article can be found online at https://doi.org/10.1016/j.clay.2022.106793.

References

Appelo, C.A.J., 1977. Chemistry of water expelled from compacting clay layers: a model based on Donnan equilibrium. Chem. Geol. 19, 91–98.
Bao, Z., Haberer, C.M., Maier, U., Amos, R.T., Blowes, D.W., Gratwohl, P., 2017. Modeling controls on the chemical weathering of marine mudrocks from the Middle Jurassic in Southern Germany. Chem. Geol. 459, 1–12.
Becker, A., Piepjohn, K., Schröder-Ritzrau, A., 2020. The Erdmannshöhle near Hasel, SW Germany: karst environment and cave evolution. Swiss J. Geosci. 113 https://doi.org/10.1186/s00015-020-00363-5.
Bleyen, N., Smets, S., Small, J., Moors, H., Leys, N., Albrecht, A., De Cannière, P., Schwyn, B., Wittebroodt, C., Valcke, E., 2017. Impact of the electron donor on in situ microbial nitrate reduction in Opalinus Clay: results from the Mont Terri rock laboratory (Switzerland). Swiss J. Geosci. 110, 355–374.
Borggaard, O.K., Lindgreen, H.B., Morup, S., 1982. Oxidation and reduction of structural iron in chlorite at 480°C. Clays Clay Min. 30, 353–364.
Delisle, G., Caspers, G., Freund, H., 2003. Permafrost in north-Central Europe during the Weichselian: How deep? In: Phillips, Springman, Arenson (Eds.), ICOP 2003 Permafrost, Proc. 8th International Conference on Permafrost, 21–25 July 2003, Zurich, Switzerland, Vol. 1. A.A. Balkema Publishers, pp. 187–191.
Dieleman, C., Christl, M., Vockenhuber, C., Gautschi, P., Graf, H.R., Akcar, N., 2022. Age of the most extensive glaciation in the Alps. Geosci. 12, 39. https://doi.org/10.3390/geosciences12010039.
Duprat-Oualid, F., 2019. 50 000 ans d'histoire de la végétation et du climat en Europe occidentale: étude pollinique et approche multi-proxy sur la séquence sédimentaire du Bergsee (Forêt Noire, Allemagne). PhD thesis. Université Bourgogne Franche-Comté, France. Available at. https://tel.archives-ouvertes.fr/tel-02338676.
Fauquette, S., Guiot, J., Menut, M., de Beaulieu, J.L., Reille, M., Guenet, P., 1999. Vegetation and climate since the last interglacial in the Vienne area (France). Glob. Planet. Chang. 20, 1–17.
Fernández, A.M., Sánchez-Ledesma, D.M., Tournassat, C., Melón, A., Gaucher, E.C., Astudillo, J., Vinsot, A., 2014. Applying the squeezing technique to highly consolidated clayrocks for porewater characterisation: Lessons learned from experiments at the Mont Terri Rock Laboratory. Appl. Geochem. 49, 2–21.
Gautschi, A., 2001. Hydrogeology of a fractured shale (Opalinus Clay): implications for deep geological disposal of radioactive wastes. Hydrogeol. J. 9, 97–107.
Giffaut, E., Grivé, M., Blanc, P., Vieillard, P., Colàs, E., Gailhanou, H., Gaboreau, S., Marty, N., Madé, B., Duro, L., 2014. Andra thermodynamic database for performance assessment: ThermoChimie. Appl. Geochem. 49, 225–236.
Giger, S.B., Marschall, P., Lanyon, G.W., Martin, C.D., 2015. Transferring the geomechanical behaviour of Opalinus Clay observed in lab tests and Mont Terri URL to assess engineering suitability at potential repository sites. In: 49th US Rock Mechanics/Geomechanics Symposium, OnePetro. ARMA, pp. 15–57.
Gimmi, T., Leupin, O., Eikenberg, J., Glaus, M.A., Van Loon, L.R., Waber, H.N., Wersin, P., Wang, H.A.O., Grolimund, D., Borca, C.N., Dewonck, S., Wittebroodt, C., 2014. Anisotropic diffusion at the field scale – I: a four-year multi-tracer diffusion and retention experiment at the Mont Terri URL (Switzerland). Geochim. Cosmochim. Acta 125, 373–393.
Hekel, U., 1994. Hydrogeologische Erkundung am Beispiel des Opalinustons (Unteres Aalenium). Tübinger geowissenschaftliche Arbeiten C18. Univ. Tübingen, Germany.
Israelachvili, J. (Ed.), 1991. Intermolecular and Surface Forces, 2nd ed. Acad. Press, New York.
Keller, O., Krayss, E., 2010. Mittel- und spätpleistozäne Stratigraphie und Morphogenese in Schlüsselregionen der Nordschweiz. Quaternary Sci. J. 59, 88–119.
Kelly, M.A., Buoncristiani, J.F., Schlüchter, C., 2004. A reconstruction of the last glacial maximum (LGM) ice-surface geometry in the western Swiss Alps and contiguous Alpine regions in Italy and France. Eclogae Geol. Helv. 97, 57–75.
Lauper, B., Zimmerli, G.N., Jaeggi, D., Deplazes, G., Wohlwend, S., Rempfer, J., Foubert, A., 2021. Quantification of lithological heterogeneity within Opalinus Clay: toward a uniform subfacies classification scheme using a novel automated core image recognition tool. Front. Earth Sci. 9, 645596 https://doi.org/10.3389/feart.2021.645596.
Le Meur, M., Boussafir, M., Le Milbeau, C., Debure, M., Claret, F., Robinet, J.C., Lerouge, C., 2021. Organic matter oxidation of the Tégulines Clay formation, (Paris Basin, France): Spatial heterogeneities. Appl. Geochem. 134 https://doi.org/10.1016/j.apgeochem.2021.105093.
Lerouge, C., Robinet, J.C., Debure, M., Tournassat, C., Bouchet, A., Fernández, A.M., Flehoc, C., Guerrot, C., Kars, M., Lagroix, F., Landrein, P., Madé, B., Negrel, P., Wille, G., Claret, F., 2018. A deep alteration and oxidation profile in a shallow clay aquitard: example of the Tégulines Clay, East Paris Basin, France. Geofluids 2018. https://doi.org/10.1155/2018/1606753.
Li, Y.H., Gregory, S., 1974. Diffusion of ions in sea water and in deep-sea sediments. Geochim. Cosmochim. Acta 38, 703–714.
Lichtner, P.C., 2004. Flotran User's Manual: Two Phase, Non-isothermal Coupled Thermal-Hydrologic-Chemical (THC) Reactive Flow and Transport Code.. LANL Rep. LA-UR-01-2349 Los Alamos National Laboratory, Los Alamos, NM, USA.
Lisiecki, L.E., Raymo, M.E., 2005. A Plio-Pleistocene stack of 57 globally distributed benthic ^{18}O records. Paleoceanography 20, PA1003. https://doi.org/10.1029/2004PA001071.
Mäder, U., Mazurek, M., 1998. Oxidation phenomena and processes in Opalinum Clay: evidence from the excavation-disturbed zones in Hauenstein and Mt. Terri tunnels, and Siblingen open clay pit. Mater. Res. Soc. Symp. Proc. 506, 731–739.
Mazurek, M., 2011. Aufbau und Auswertung der Gesteinsparameter-Datenbank für Opalinuston, den Braunen Dogger , Effinger Schichten und Mergel-Formationen des Helvetikums. Nagra Arbeitsbericht NAB 11–20, Nagra, Wettingen, Switzerland. Available at. www.nagra.ch.
Mazurek, M., Alexander, W.R., MacKenzie, A.B., 1996. Contaminant retardation in fractured shales: Matrix diffusion and redox front entrapment. J. Contam. Hydrol. 21, 71–84.
Mazurek, M., Hurford, A.J., Leu, W., 2006. Unravelling the multi-stage burial history of the Swiss Molasse Basin: Integration of apatite fission track, vitrinite reflectance and biomarker isomerisation analysis. Basin Res. 18, 27–50.

Mazurek, M., Alt-Epping, P., Bath, A., Gimmi, T., Waber, H.N., Buschaert, S., De Cannière, P., De Craen, M., Gautschi, A., Savoye, S., Vinsot, A., Wemaere, I., Wouters, L., 2011. Natural tracer profiles across argillaceous formations. Appl. Geochem. 26, 1035–1064.

Mazurek, M., Oyama, T., Wersin, P., Alt-Epping, P., 2015. Pore-water squeezing from indurated shales. Chem. Geol. 400, 106–121.

Mazurek, M., Wersin, P., Hadi, J., Baeyens, B., Dohrmann, R., Grenèche, J.M., Marques, M., Oyama, T., Rufer, D., Waber, H.N., 2017a. Opalinus Clay in the shallow decompaction zone: Geochemical investigations on drill core samples from borehole Lausen KB. Nagra Arbeitsbericht NAB 16–58, Nagra, Wettingen, Switzerland. Available at. www.nagra.ch.

Mazurek, M., Al, T., Celejewski, M., Clark, I.D., Fernandez, A.M., Jäggi, D., Kennell-Morrison, L., Matray, J.M., Murseli, S., Oyama, T., Qiu, S., Rufer, D., St-Jean, G., Waber, H.N., Yu, C., 2017b. Mont Terri DB-A Experiment: Comparison of Pore-water Investigations Conducted by Several Research Groups on Core Materials from the BDB-1 Borehole. Mont Terri Technical Report 17–01, Mont Terri Project, Switzerland, and Technical Report NWMO-TR-2017-09. Nuclear Waste Management Organization, Toronto, Canada. Available at nwmo.ca.

Mazurek, M., Aschwanden, L., Camesi, L., Gimmi, T., Jenni, A., Kiczka, M., Mäder, U., Rufer, D., Waber, H.N., Wanner, P., Wersin, P., Traber, D., 2021. TBO Bülach-1-1: Data Report. Dossier VIII – Rock Properties, Porewater Characterisation and Natural Tracer Profiles. Nagra Arbeitsbericht NAB 20–08, Nagra, Wettingen, Switzerland.. Available at. www.nagra.ch.

Mertens, J., Vandenberghe, N., Wouters, L., Sintubin, M., 2003. The origin and development of joints in the Boom Clay Formation (Rupelian) in Belgium. In: Van Rensbergen, P., Hillis, R.R., Maltman, A.J., Morley, C.K. (Eds.), Subsurface sediment mobilization, 216. Geol. Soc. London, Spec. Publ., pp. 309–321

Nagra, 2014. SGT Etappe 2: Vorschlag weiter zu untersuchender geologischer Standortgebiete mit zugehörigen Standortarealen für die Oberflächenanlage – Dossier VI: Barriereneigenschaften der Wirt- und Rahmengesteine. Nagra Technischer Bericht 14–02. Nagra, Wettingen, Switzerland. Available at. www.nagra.ch.

NEA, 2009. In: Considering timescales in the post-closure safety of geological disposal of radioactive waste. NEA No. 6224. OECD Nuclear Energy Agency, Paris, France.

Neuzil, C.E., 1994. How permeable are clays and shales? Water Resour. Res. 30, 145–150.

Neuzil, C.E., 2019. Permeability of Clays and Shales. Annu. Rev. Earth Planet. Sci. 47, 247–273.

Parkhurst, D.L., Appelo, C.A.J., 2013. Description of input and examples for PHREEQC version 3 – a computer program for speciation, batch-reaction, one-dimensional transport, and inverse geochemical calculations. In: US Geological Survey Techniques and Methods book 6, ch. A43. Available at. http://pubs.usgs.gov/tm/06/a43.

Pearson, F.J., Balderer, W., Loosli, H.H., Lehmann, B.E., Matter, A., Peters, T., Schmassmann, H., Gautschi, A., 1991. Applied isotope hydrogeology – a case study in northern Switzerland. Stud. Environ. Sci. 43. Elsevier.

Pearson, F.J., Arcos, D., Bath, A., Boisson, J.Y., Fernández, A.M., Gäbler, H.E., Gaucher, E., Gautschi, A., Griffault, L., Hernán, P., Waber, H.N., 2003. Mont Terri Project – Geochemistry of Water in the Opalinus Clay Formation at the Mont Terri Rock Laboratory: Bern, 5. Federal Office for Water and Geology (FOWG), Switzerland. Geology Series.

Pearson, F.J., Tournassat, C., Gaucher, E.C., 2011. Biogeochemical processes in a clay formation in situ experiment: Part E – Equilibrium controls on chemistry of pore water from the Opalinus Clay, Mont Terri Underground Research Laboratory, Switzerland. Appl. Geochem. 26, 990–1008.

Pekala, M., Wersin, P., Rufer, D., Curti, E., 2018. Mineralogy of carbonate and sulphate minerals in the Opalinus Clay and adjacent formations. Mont Terri Technical Report TR 2018-03. Mont Terri Project, Switzerland. Available at. mont-terri.ch.

Preusser, F., Graf, H.R., Keller, O., Krayss, E., Schlüchter, C., 2011. Quaternary glaciation history of northern Switzerland. Quaternary Sci. J. 60, 282–305.

Rübel, A., Sonntag, C., Lippmann, J., Pearson, F.J., Gautschi, A., 2002. Solute transport in formations of very low permeability: Profiles of stable isotope and dissolved noble gas contents of pore water in the Opalinus Clay, Mont Terri, Switzerland. Geochim. Cosmochim. Acta 66, 1311–1321.

Stevens, J.G., Khasanov, A.M., Miller, J.W., Pollak, H., Li, Z., 2005. Mössbauer Mineral Handbook. MEDC.

Van Loon, L.R., Mibus, J., 2015. A modified version of Archie's law to estimate effective diffusion coefficients of radionuclides in argillaceous rocks and its application in safety analysis studies. Appl. Geochem. 59, 85–94.

Van Loon, L.R., Soler, J.M., 2003. Diffusion of HTO, $^{36}Cl^-$, $^{125}I^-$ and $^{22}Na^+$ in Opalinus Clay: Effect of confining pressure, sample orientation, sample depth and temperature. Nagra Technical Report NTB 03–07. Nagra, Wettingen, Switzerland. Available at www.nagra.ch.

Van Loon, L.R., Müller, W., Iijima, K., 2005a. Activation energies of the self-diffusion of HTO, $^{22}Na^+$ and $^{36}Cl^-$ in a highly compacted argillaceous rock (Opalinus Clay). Appl. Geochem. 20, 961–972.

Van Loon, L.R., Baeyens, B., Bradbury, M.H., 2005b. Diffusion and retention of sodium and strontium in Opalinus clay: Comparison of sorption data from diffusion and batch sorption measurements, and geochemical calculations. Appl. Geochem. 20, 2351–2363.

Vinsot, A., Appelo, C.A.J., Cailteau, C., Wechner, S., Pironon, J., De Donato, P., De Cannière, P., Mettler, S., Wersin, P., Gäbler, H.E., 2008. CO_2 data on gas and porewater sampled in situ in the Opalinus Clay at the Mont Terri rock laboratory. Phys. Chem. Earth 33, S54–S60.

Vinsot, A., Appelo, C.A.J., Lundy, M., Wechner, S., Lettry, Y., Lerouge, C., Fernandez, A. M., Labat, M., Tournassat, C., De Cannière, P., Schwyn, B., McKelvie, J., Dewonck, S., Bossart, P., Delay, J., 2014. In situ diffusion test of hydrogen gas in the Opalinus Clay. In: Norris, S., Bruno, J., Cathelineau, M., Delage, P., Fairhurst, C., Gaucher, E.C., Hoehn, E.H., Kalinichev, A., Lalieux, P., Sellin, P. (Eds.), Clays in Natural and Engineered Barriers for Radioactive Waste Confinement, 400. Geol. Soc. London Spec. Publ. https://doi.org/10.1144/SP400.12

Vogt, T., Ebert, A., Häring, C., Becker, J.K., Traber, D., Bläsi, H.R., Rufer, D., 2016. Kernbohrung Lausen: Geologische, hydrogeologische und bohrlochgeophysikalische Untersuchungen (Rohdatenbericht). Nagra Arbeitsbericht NAB 15–10. Nagra, Wettingen, Switzerland. Available at www.nagra.ch.

Vogt, T., Hekel, U., Ebert, A., Becker, J.K., Traber, D., Giger, S., Brod, M., Häring, C., 2017. Hydrogeologische Untersuchungen im oberflächennahen Opalinuston. Grundwasser, Bohrloch Lausen Schweiz. https://doi.org/10.1007/s00767-017-0363-2.

Waber, H.N., Heidinger, M., Lorenz, G., Traber, D., 2014. Hydrochemie und Isotopenhydrogeologie von Tiefengrundwässern in der Nordschweiz und im angrenzenden Süddeutschland. Nagra Arbeitsbericht NAB 13–63. Nagra, Wettingen, Switzerland. Available at.

Wersin, P., Baeyens, B., Bossart, P., Cartalade, A., Dewonck, S., Eikenberg, J., Fierz, T., Fisch, H.R., Gimmi, T., Grolimund, D., Hernan, P., Möri, A., Savoye, S., Soler, J., van Dorp, F., Van Loon, L., 2006. Long-Term Diffusion Experiment (DI-A): Diffusion of HTO, I^-, $^{22}Na^+$ and Cs: Field Activities, Data and Modelling. Mont Terri Technical Report TR 03-06.. Mont Terri Project, Switzerland.

Wersin, P., Appelo, C.A.J., Baeyens, B., Bossart, P., Dewonck, S., Eikenberg, J., Fierz, T., Fisch, H.R., Gimmi, T., Grolimund, D., Leupin, O.X., Möri, A., Soler, J.M., van Dorp, F., Van Loon, L.R., 2010. Long-Term Diffusion (DI-A) Experiment: DI-A2: Diffusion of HTO, Br^-, I-, Cs^+, $^{85}Sr^{2+}$ and $^{60}Co^{2+}$: Field Activities, Data and Modelling. Mont Terri Technical Report TR 09-04. Mont Terri Project, Switzerland.

Wersin, P., Pekala, M., Mazurek, M., Gimmi, T., Mäder, U., Jenni, A., Rufer, D., Aschwanden, L., 2020. Porewater Chemistry of Opalinus Clay: Methods, Data, Modelling & Buffering Capacity. Nagra Technical Report NTB 18–01, Nagra, Wettingen, Switzerland. Available at. www.nagra.ch.

Wersin, P., Mazurek, M., Gimmi, T., 2022. Porewater chemistry of Opalinus Clay revisited: Findings from 25 years of data collection at the Mont Terri Rock Laboratory. Appl. Geochem. 138 https://doi.org/10.1016/j.apgeochem.2022.105234.

Wetzel, A., Allia, V., 2003. Der Opalinuston in der Nordschweiz: Lithologie und Ablagerungsgeschichte. Eclogae Geol. Helv. 96, 451–469.

Wetzel, A., Einsele, G., 1991. On the physical weathering of various mudrocks. Bull. Internat. Assoc. Eng. Geol. 44, 89–100.

Yu, C., Matray, J.M., Gonçalvès, J., Jäggi, D., Gräsle, W., Wieczorek, K., Vogt, T., Sykes, E., 2017. Comparative study of methods to estimate hydraulic parameters in the hydraulically undisturbed Opalinus Clay (Switzerland). Swiss J. Geosci. 110, 85–104. https://doi.org/10.1007/s00015-016-0257-9.